Full analytical model for obtaining surface plasmon resonance modes of metal nanoparticle structures embedded in layered media

Ergun Simsek

Electrical and Electronics Engineering,
Bahcesehir University, Istanbul, TURKEY
ergun.simsek@bahcesehir.edu.tr

Abstract: This work addresses the need for a fully-retarded theoretical model for surface plasmons on metal nanoparticle chains and arrays embedded in a multilayered medium. The proposed method uses dyadic layered medium Green's functions not only to obtain the electric field created by an oscillating electric dipole but also to modify the polarizability of nanoparticles in a multilayered medium appropriately. Theoretically calculated resonance frequencies show a very good agreement with the experimental results found in the literature. Theoretical results suggest that surface plasmon propagation lengths of 1 μm are possible using silver or gold nanoparticles embedded in a multilayered medium.

OCIS codes: (240.6680) Surface Plasmons; (230.4555) Coupled Resonators.

References and links

1. K. B. Crozier, A. Sundaramurthy, G. S. Kino, and C. F. Quate, "Optical antennas: Resonators for local field enhancement," J. Appl. Phys. **94**, 4632–4642 (2003).
2. E. Hao and G. C. Schatz, "Electromagnetic fields around silver nanoparticles and dimers," J. Chem. Phys. **120**, 357–366 (2004).
3. S. L. Zou and G. C. Schatz, "Silver nanoparticle array structures that produce giant enhancements in electromagnetic fields," Chem. Phys. Lett. **403**, 62–67 (2005).
4. A. Sundaramurthy, K. B. Crozier, G. S. Kino, D. P. Fromm, P. J. Schuck, and W. E. Moerner, "Field enhancement and gap-dependent resonance in a system of two opposing tip-to-tip au nanotriangles," Phys. Rev. B **72**, 165409 (2005).
5. E. Cubukcu, E. A. Kort, K. B. Crozier, and F. Capasso, "Plasmonic laser antenna," Appl. Phys. Lett. **89**, 093120 (2006).
6. M. Guillon, "Field enhancement in a chain of optically bound dipoles," Opt. Express **14**, 3045–3055 (2006).
7. K. Kneipp, Y. Wang, H. Kneipp, L. T. Perelman, I. Itzkan, R. R. Dasari, and M. S. Feld, "Single molecule detection using surface-enhanced raman scattering (sers)," Phys. Rev. Lett. **78**, 1667–1670 (1997).
8. K. Kneipp, H. Kneipp, I. Itzkan, R. R. Dasari, and M. S. Feld, "Surface-enhanced raman scattering and biophysics," J. Phys. Cond. Matter **14**, R597–R624 (2002).
9. N. Félidj, J. Aubard, G. Lévi, J. R. Krenn, M. Salerno, G. Schider, B. Lamprecht, A. Leitner, and F. R. Aussenegg, "Controlling the optical response of regular arrays of gold particles for surface-enhanced raman scattering," Phys. Rev. B **65**, 075419 (2002).
10. N. Félidj, S. L. Truong, J. Aubard, G. Lévi, J. R. Krenn, A. Hohenau, A. Leitner, and F. R. Aussenegg, "Gold particle interaction in regular arrays probed by surface enhanced raman scattering," J. Chem. Phys. **120**, 7141–7146 (2004).

#121182 - $15.00 USD Received 8 Dec 2009; revised 4 Jan 2010; accepted 11 Jan 2010; published 14 Jan 2010

11. J. Grand, M. L. de la Chapelle, J.-L. Bijeon, P.-M. Adam, A. Vial, and P. Royer, "Role of localized surface plasmons in surface-enhanced raman scattering of shape-controlled metallic particles in regular arrays," Phys. Rev. B **72**, 033407 (2005).
12. G. Laurent, N. Félidj, J. Aubard, G. Lévi, J. R. Krenn, A. Hohenau, G. Schider, A. Leitner, and F. R. Aussenegg, "Evidence of multipolar excitations in surface enhanced raman scattering," Phys. Rev. B **71**, 045430 (2005).
13. D. P. Fromm, A. Sundaramurthy, A. Kinkhabwala, P. J. Schuck, G. S. Kino, and W. E. Moerner, "Exploring the chemical enhancement for surface-enhanced raman scattering with au bowtie nanoantennas," J. Chem. Phys. **124**, 061101 (2006).
14. K. H. Su, S. Durant, J. M. Steele, Y. Xiong, C. Sun, and X. Zhang, "Wavelength-scanned surface-enhanced raman excitation spectroscopy," Phys. Chem B **110**, 3964–3968 (2006).
15. B. Pettinger, B. Ren, G. Picardi, R. Schuster, and G. Ertl, "Nanoscale probing of adsorbed species by tip-enhanced raman spectroscopy," Phys. Rev. Lett. **92**, 096101 (2004).
16. R. M. Stöckle, Y. D. Suh, V. Deckert, and R. Zenobi, "Nanoscale chemical analysis by tip-enhanced raman spectroscopy," Chem. Phys. Lett. **318**, 131–136 (2000).
17. S. Pillai, K. R. Catchpole, T. Trupke, and M. A. Green, "Surface plasmon enhanced silicon solar cells," J. Appl. Phys. **101**, 093105 (2007).
18. K. R. Catchpole and A. Polman, "Plasmonic solar cells," Opt. Express **16**, 21793–21800 (2008).
19. M. Danckwerts and L. Novotny, "Optical frequency mixing at coupled gold nanoparticles," Phys. Rev. Lett. **98**, 026104 (2007).
20. K. H. Su, Q. H. Wei, X. Zhang, J. J. Mock, D. R. Smith, and S. Schultz, "Interparticle coupling effects on plasmon resonances of nanogold particles," Nano Lett. **3**, 1087–1090 (2003).
21. G. Schider, J. R. Krenn, A. Hohenau, H. Ditlbacher, A. Leitner, F. R. Aussenegg, W. L. Schaich, I. Puscasu, B. Monacelli, and G. Boreman, "Plasmon dispersion relation of au and ag nanowires," Phys. Rev. B **68**, 155427 (2003).
22. K. L. Kelly, E. Coronado, L. L. Zhao, and G. C. Schatz, "The optical properties of metal nanoparticles: The influence of size, shape, and dielectric environment," J Phys Chem B **107**, 668–677 (2003).
23. L. J. Sherry, R. Jin, C. A. Mirkin, G. C. Schatz, and R. P. Van Duyne, "Localized surface plasmon resonance spectroscopy of single silver triangular nanoprisms," Nano Lett. **6** (2006).
24. M. D. Malinsky, K. L. Kelly, G. C. Schatz, and R. P. V. Duyne, "Nanosphere lithography: Effect of substrate on the localized surface plasmon resonance spectrum of silver nanoparticles," J. Phys. Chem. B **105**, 2343–2350 (2001).
25. W. Rechberger, A. Hohenau, A. Leitner, J. Krenn, B. Lamprecht, and F. Aussenegg, "Optical properties of two interacting gold nanoparticles," Opt. Commun. **220**, 137–141 (2003).
26. C. Noguez, "Surface plasmons on metal nanoparticles: The influence of shape and physical environment," J. Phys. Chem. C **111**, 3806–3819 (2007).
27. V. Markel, "Coupled-dipole approach to scattering of light from a one-dimensional periodic dipole structure," J. Mod. Opt. **40**, 2281–2291 (1993).
28. S. Maier, P. Kik, and H. Atwater, "Observation of coupled plasmon-polariton modes in au nanoparticle chain waveguides of different lengths: Estimation of waveguide loss," Appl. Phys. Lett. **81**, 1714–1716 (2002).
29. J. Takahara, S. Yamagishi, H. Taki, A. Morimoto, and T. Kobayashi, "Guiding of a one-dimensional optical beam with nanometer diameter," Opt. Lett. **22**, 475–477 (1997).
30. M. Quinten, A. Leitner, J. R. Krenn, and F. R. Aussenegg, "Electromagnetic energy transport via linear chains of silver nanoparticles," Opt. Lett. **23**, 1331–1333 (1998).
31. S. A. Maier, M. L. Brongersma, P. G. Kik, and H. A. Atwater, "Observation of near-field coupling in metal nanoparticle chains using far-field polarization spectroscopy," Phys. Rev. B **65**, 193408 (2002).
32. S. Y. Park and D. Stroud, "Surface-plasmon dispersion relations in chains of metallic nanoparticles: An exact quasistatic calculation," Phys. Rev. B **69**, 125418 (2004).
33. M. I. Stockman, K. Li, and D. J. Bergman, "Self-similar chain of metal nanospheres as efficient nanolens," in "Conference on Lasers and Electro-Optics/International Quantum Electronics Conference and Photonic Applications Systems Technologies," (Optical Society of America, 2004), p. IFC2.
34. R. Quidant, C. Girard, J.-C. Weeber, and A. Dereux, "Tailoring the transmittance of integrated optical waveguides with short metallic nanoparticle chains," Phys. Rev. B **69**, 085407 (2004).
35. S. Zou and G. C. Schatz, "Theoretical studies of plasmon resonances in one-dimensional nanoparticle chains: narrow lineshapes with tunable widths," Nanotechnology **17**, 2813–2820 (2006).
36. C. R. Simovski, A. J. Viitanen, and S. A. Tretyakov, "Resonator mode in chains of silver spheres and its possible application," Phys. Rev. E **72**, 066606 (2005).
37. W. H. Weber and G. W. Ford, "Propagation of optical excitations by dipolar interactions in metal

#121182 - $15.00 USD Received 8 Dec 2009; revised 4 Jan 2010; accepted 11 Jan 2010; published 14 Jan 2010

nanoparticle chains," Phys. Rev. B **70**, 125429 (2004).
38. A. F. Koenderink and A. Polman, "Complex response and polariton-like dispersion splitting in periodic metal nanoparticle chains," Phys. Rev. B **74**, 033402 (2006).
39. A. F. Koenderink, R. de Waele, J. C. Prangsma, and A. Polman, "Experimental evidence for large dynamic effects on the plasmon dispersion of subwavelength metal nanoparticle waveguides," Phys. Rev. B **76**, 201403 (2007).
40. K. Crozier, E. Togan, E. Simsek, and T. Yang, "Experimental measurement of the dispersion relations of the surface plasmon modes of metal nanoparticle chains," Opt. Express **16**, 13070 (2008).
41. E. Simsek, "On the surface plasmon resonance modes of metal nanoparticle chains and arrays," Plasmonics **4**, 223–230 (2009).
42. M. L. Brongersma, J. W. Hartman, and H. A. Atwater, "Electromagnetic energy transfer and switching in nanoparticle chain arrays below the diffraction limit," Phys. Rev. B **62**, R16356–R16359 (2000).
43. B. Lamprecht, G. Schider, R. T. Lechner, H. Ditlbacher, J. R. Krenn, A. Leitner, and F. R. Aussenegg, "Metal nanoparticle gratings: Influence of dipolar particle interaction on the plasmon resonance," Phys. Rev. Lett. **84**, 4721–4724 (2000).
44. C. L. Haynes, A. D. McFarland, L. Zhao, R. P. V. Duyne, G. C. Schatz, L. Gunnarsson, J. Prikulis, B. Kasemo, and M. Kall, "Nanoparticle optics: The importance of radiative dipole coupling in two-dimensional nanoparticle arrays," J. Phys. Chem. B **107**, 7337–7342 (2003).
45. S. Zou and G. C. Schatz, "Narrow plasmonic/photonic extinction and scattering line shapes for one and two dimensional silver nanoparticle arrays," J. Chem. Phys. **121**, 12606–12612 (2004).
46. E. J. Smythe, E. Cubukcu, and F. Capasso, "Optical properties of surface plasmon resonances of coupled metallic nanorods," Opt. Express **15**, 7439–7447 (2007).
47. Y. Chu, E. Schonbrun, T. Yang, and K. B. Crozier, "Experimental observation of narrow surface plasmon resonances in gold nanoparticle arrays," Appl. Phys. Lett. **93**, 181108 (2008).
48. B. Auguie and W. L. Barnes, "Collective resonances in gold nanoparticle arrays," Phys. Rev. Lett. **101**, 143902 (2008).
49. T. Yang and K. B. Crozier, "Dispersion and extinction of surface plasmons in an array of gold nanoparticle chains: influence of the air/glass interface," Opt. Express **16**, 8570–8580 (2008).
50. T. Yang and K. B. Crozier, "Surface plasmon coupling in periodic metallic nanoparticle structures: a semi-analytical model," Opt. Express **16**, 13070–13079 (2008).
51. E. Bae, H. Zhang, and E. D. Hirleman, "Application of the discrete dipole approximation for dipoles embedded in film," J. Opt. Soc. Am. A **25**, 1728–1736 (2008).
52. K. A. Michalski and D. Zheng, "Electromagnetic scattering and radiation by surfaces of arbitrary shape in layered media, part i: Theory," IEEE Micr. Theo. Tech. **38**, 335 (1990).
53. W. C. Chew, *Waves and Fields in Inhomogeneous Media* (IEEE Press, Piscataway, NJ, 1995).
54. G. Dural and M. I. Aksun, "Closed form green's functions for general sources and stratified media," IEEE Trans. Micr. Theo. Tech. **43**, 1545 (1995).
55. M. Paulus, P. Gay-Balmaz, and O. J. F. Martin, "Accurate and efficient computation of the Green's tensor for stratified media," Phys. Rev. E **62**, 5797–5807 (2000).
56. M. Paulus and O. J. F. Martin, "Light propagation and scattering in stratified media: a GreenÕs tensor approach," J. Opt. Soc. Am. A **18**, 854–861 (2001).
57. E. Simsek, Q. H. Liu, and B. Wei, "Singularity subtraction for evaluation of green's functions for multilayer media," IEEE Trans. Micr. Theo. Tech. **54**, 216–225 (2006).
58. A. Sommerfeld, *Partial Differential Equations in Physics* (Academic Press, New York, 1949).
59. J. Aizpurua, T. Taubner, F. J. G. de Abajo, M. Brehm, and R. Hillenbrand, "Substrate-enhanced infrared near-fieldspectroscopy," Opt. Express **16**, 1529–1545 (2008).
60. A. D. Rakic, A. B. Djurišic, J. M. Elazar, and M. L. Majewski, "Optical properties of metallic films for vertical-cavity optoelectronic devices," Appl. Opt. **37**, 5271–5283 (1998).

1. INTRODUCTION

In the last decade, there has been a great interest in surface plasmons (SPs) due to their potential for developing new types of optical communication devices and sensors. Theoretical and experimental studies have shown that periodically placed nanoparticles (NPs) can lead to giant electromagnetic field enhancement which can be useful for detecting molecules at low concentrations [1, 2, 3, 4, 5, 6]. Applications of SPs include surface [7, 8, 9, 10, 11, 12, 13, 14] or tip [15, 16] enhanced Raman scattering, plasmonic solar cells [17, 18] and nonlinear frequency generation [19]. In these works, researchers

#121182 - $15.00 USD Received 8 Dec 2009; revised 4 Jan 2010; accepted 11 Jan 2010; published 14 Jan 2010

tune up the properties of SPs and their interaction with light for their problem of interest by changing the shape, size, and material composition of NPs [1, 2, 3, 4, 5, 6, 7, 8, 9, 10, 11, 12, 13, 14, 15, 16, 17, 18, 19, 20, 21, 22, 23, 24, 25, 26]. The specific interest of this work is the design of a full analytical model to calculate SP resonance modes of metal NP structures embedded in a multilayered medium.

Many researchers have studied SP resonance modes of NP chains [6, 27, 28, 29, 30, 31, 32, 33, 34, 35, 36, 37, 38, 39, 40, 41] and arrays [41, 3, 42, 43, 44, 45, 46, 47, 48] theoretically, numerically, and/or experimentally. Even though the accuracy of theoretical models based on the coupled dipole approximation (CDA) has been improved over the years [30, 32, 37, 38, 42], a non-negligible discrepancy between experimental and theoretical results still remains [39, 40]. The main reason behind such a difference is due to the fact that the CDA based theoretical models assume a homogeneous background, which is not the case for almost all of the fabricated structures. This is also why numerical techniques (e.g. finite difference-time domain methods) that can handle inhomogeneous backgrounds are preferred to compare with the experimental results [40, 46, 47].

One way of handling inhomogeneity is assigning an effective refractive index for the background [41], and applying homogeneous background techniques, such as CDA. This approach can provide a good estimate of SP resonance modes but can not explain the exact effect of an interface (such as air/glass interface in [49]) on the dispersion and extinction of surface plasmons. In [26, 39], researchers try to implement CDA by the help of image theory (IT) to take air/glass interface into account. Experimental results support the validity of such a theoretical model [39] but it is still unclear how IT can be implemented for structures with more than two layers, especially for the case where the width of the layer (on which NPs are aligned) is less than the half of the height of NPs.

Yang and Crozier propose a semi-analytical model for NPs on top of a glass slide [50] and show good agreement between their model and experimental results for the first transverse mode. Up to our knowledge, this is the first CDA based model, which can describe the effect of the air/glass interface. The main advantage of their model is that it only involves real valued frequencies. The drawback, however, is the requirement of a full wave solver in order to calculate the polarizability of NPs. In this work, we overcome this requirement by appropriately modifying the polarizability factor using layered medium Green's functions (LMGFs). We also implement CDA with LMGFs and hence obtain a full analytical model that can accurately calculate SP resonance modes of metal NP structures embedded in a multilayered medium. This fully retarded theoretical model includes the effects of retardation, radiative damping, and dynamic depolarization due to the finite size of NPs based on the Modified Long Wavelength Approximation (MLWA) [22]. Unlike [51], the formulation is not limited to three-layer media.

The outline of this paper is as follows. We first briefly explain how to evaluate LMGFs. Then we implement LMGFs (i) to calculate the polarizability of the NPs embedded in a layered medium and (ii) to extend CDA to layered media. Finally, we present numerical results, which show a good agreement with experimental data and support the experimental observations described in [40] about the existence of the second transverse mode. Propagation lengths (PLs) of each mode are also calculated.

#121182 - $15.00 USD Received 8 Dec 2009; revised 4 Jan 2010; accepted 11 Jan 2010; published 14 Jan 2010

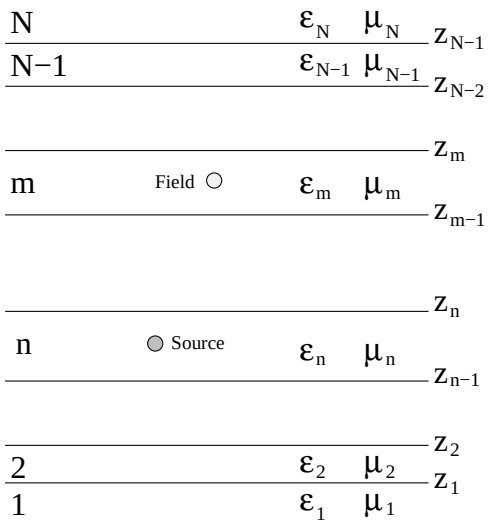

Fig. 1. An N-layer medium with source and field points in layer n and layer m,respectively.

2. Layered Medium Green's Functions

Consider a general multilayer medium consisting of N layers separated by $N-1$ planar interfaces parallel to the xy plane, as shown in Figure 1. Layer i exists between z_i and z_{i-1} and is characterized by permittivity ε_i and permeability μ_i. An arbitrarily directed electric dipole $\mathbf{p}$ can be represented in the cartesian coordinates by $\mathbf{p} = \hat{\mathbf{x}}p_x + \hat{\mathbf{y}}p_y + \hat{\mathbf{z}}p_z$. Similarly, electric field $\mathbf{E}$ created by that dipole can be decomposed as $\mathbf{E} = \hat{\mathbf{x}}E_x + \hat{\mathbf{y}}E_y + \hat{\mathbf{z}}E_z$. The relationship between each component of the field and the dipole is given by the dyadic layered medium Green's functions, $\bar{G}(\mathbf{r},\mathbf{r}')$, as follows

$$\begin{bmatrix} E_x \\ E_y \\ E_z \end{bmatrix} = \begin{bmatrix} G_{xx} & G_{xy} & G_{xz} \\ G_{yx} & G_{yy} & G_{yz} \\ G_{zx} & G_{zy} & G_{zz} \end{bmatrix} . \begin{bmatrix} p_x \\ p_y \\ p_z \end{bmatrix} . \tag{1}$$

In this notation, $G_{\eta\zeta}$ gives $\hat{\eta}$ component of the electric field at $\mathbf{r}$ due to a $\hat{\zeta}$ directed unit electric dipole located at $\mathbf{r}'$, where η and ζ are either x, y, or z.

As a first step to calculate LMGFs, the problem is transformed from spatial domain to spectral domain. Each layer is represented by a uniform transmission line having the same physical properties; hence electric and magnetic fields can be interpreted as voltage and current, respectively, on a transmission line [52, 53]. By using this transmission line analogy, Green's functions in spectral domain, called transmission line Green's functions, can be calculated in compact form. The spectral domain counter parts of the

#121182 - $15.00 USD Received 8 Dec 2009; revised 4 Jan 2010; accepted 11 Jan 2010; published 14 Jan 2010

diagonal components are given by

$$\tilde{G}_{xx} = \frac{k_x^2}{k_\rho^2}\tilde{G}^{TM,VI} + \frac{k_y^2}{k_\rho^2}\tilde{G}^{TE,VI},$$
$$\tilde{G}_{yy} = \frac{k_x^2}{k_\rho^2}\tilde{G}^{TE,VI} + \frac{k_y^2}{k_\rho^2}\tilde{G}^{TM,VI}, \tag{2}$$
$$\tilde{G}_{zz} = \frac{k_\rho^2}{\omega^2\varepsilon_i\varepsilon_m}\tilde{G}^{TM,IV},$$

where subscripts i and m represent source and field layers, respectively; $\tilde{G}^{h,PQ}$ is the transmission line Green's function, which represents voltage or current (P) due to a voltage or current source (Q) for either TE or TM case (h); k_η is the wavenumber along $\hat{\eta}$; ω is the radial frequency. The complete expressions for transmission line Green's functions can be found in [52, 53, 54, 55, 56, 57].

The spatial domain LMGF is the inverse transformation from spectral domain to spatial domain and is known as a Sommerfeld integral [58] given by

$$G_{\eta\zeta}(\rho, z|z') = \frac{1}{2\pi}\int_0^\infty \tilde{G}_{\eta\zeta}(\mathbf{k}_\rho, z|z')J_\nu(k_\rho\rho)k_\rho^{\nu+1}dk_\rho \tag{3}$$

where $\nu = 0, 1$, J_ν is ν^{th} order Bessel function, $\rho = \sqrt{(x-x')^2+(y-y')^2}$ and $\tilde{G}_{\eta\zeta}(\mathbf{k}_\rho, z|z')$ is its spectral domain counterpart.

It should be noted that LMGF's can be written as a sum of primary field term and reflection terms:

$$G_{\eta\zeta} = G_{\eta\zeta}^{prim} + G_{\eta\zeta}^{refl}. \tag{4}$$

The primary field term, the direct interaction between the source and field, can be calculated directly by using Sommerfeld identity [58]. The contribution of the reflections is calculated by taking the integral given in (3). In order to accelerate this process, the singular terms of the integrand are subtracted and their contribution is calculated analytically, as explained in [57]. The remaining integral is computed numerically by using Gaussian quadratures.

3. Layered Medium CDA

The dispersion relations are obtained as described in [37]. Assume there is a finite chain of equally spaced metal NPs along the $\hat{x}$-axis in a multilayered medium; M is the number of NPs and d is the inter-particle spacing. Again assume NPs can be represented as oscillating dipoles ($\mathbf{p_j}$, $j = 1, 2, \cdots, M$) and ω is the oscillating frequency in the absence of an applied field. Note that treatment of nanoparticles as point dipoles means the results are valid only for $3a < d$, where a is the particle radius. The induced dipole moment on particle-n because of field generated by dipole-m can be calculated as

$$\mathbf{p}_n = \bar{G}(\mathbf{r_n}, \mathbf{r_m}) \begin{bmatrix} \alpha_x(\omega) & 0 & 0 \\ 0 & \alpha_y(\omega) & 0 \\ 0 & 0 & \alpha_z(\omega) \end{bmatrix} \mathbf{p_m}, \tag{5}$$

where $\alpha_\eta(\omega)$ is frequency dependent polarizability of NP along the $\hat{\eta}$-direction.

Surface plasmon resonance occurs when the dipole moment of a single NP becomes equal to the induced dipole moment on that NP due to all other dipoles. Using (5) and the fact that any vector in 3-dimensional space can be written as a combination

#121182 - $15.00 USD Received 8 Dec 2009; revised 4 Jan 2010; accepted 11 Jan 2010; published 14 Jan 2010

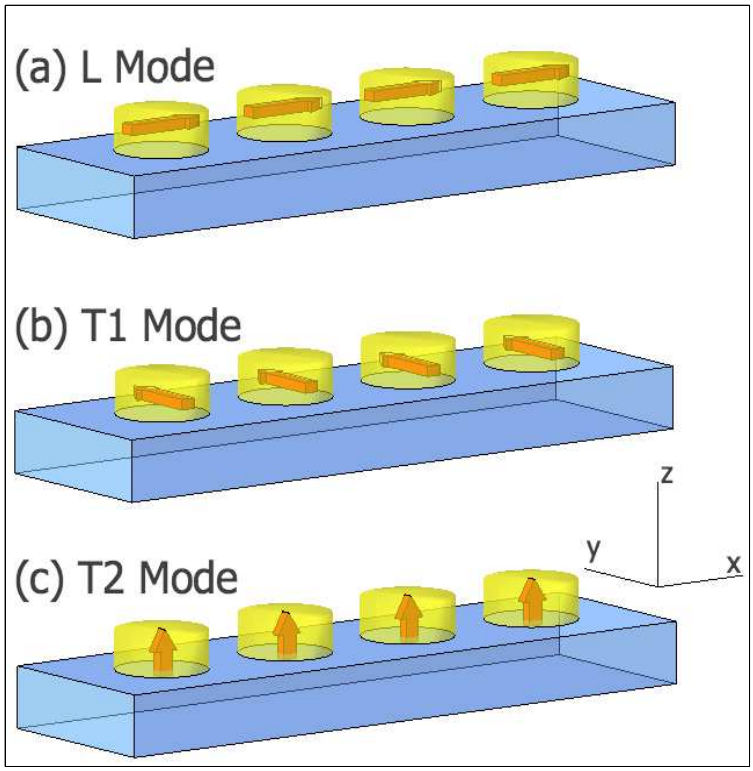

Fig. 2. Induced moments (red arrows) inside metal NPs (yellow cylinders) on top of a substrate (blue rectangular cubes): for **(a)** longitudinal, **(b)** transverse-1, **(c)** transverse-2 modes. The inter-particle spacing is d along $\hat{\mathbf{x}}$-axis.

of 3 orthogonal unit vectors, we can generate three independent dispersion modes: one longitudinal and two transverse modes. Fig. 2 shows these three cases: dipoles are parallel to (a) $\hat{x}$-axis, (b) $\hat{y}$-axis, (c) $\hat{z}$-axis. Hence, we obtain three dispersion relations:

$$1 - \alpha_\eta(\omega) \sum_{n=1}^{M-1} G_{\eta\eta}(\mathbf{r_0}, \mathbf{r_n}) = 0, \tag{6}$$

where $\mathbf{r_n} = nd\hat{\mathbf{x}}$, assuming $\mathbf{r_0}$ is located at the origin; $\eta = x$ for the longitudinal mode (L), $\eta = y$ for the first transverse mode ($T1$), $\eta = z$ for the second transverse mode ($T2$). For a chain of M metal NPs, Eq. (6) becomes a set of M coupled equations in the M unknown moments of NPs. One can put these equations in a matrix form as explained in [37] and calculate resonance frequencies for which the matrix coupling the dipoles is singular. Then these frequencies are mapped onto the dispersion relations appropriate for the infinite chain. For the complete procedure, reader is kindly referred to [37].

Replacing the free space Green's functions with layered medium Green's functions is not enough to extend CDA to layered media; the polarizability of NP should be handled appropriately as well. Assume that we deal with ellipsoidal metal NPs on the xy-plane.

#121182 - $15.00 USD Received 8 Dec 2009; revised 4 Jan 2010; accepted 11 Jan 2010; published 14 Jan 2010

The semi-axes (r_η) of the ellipsoids along the (x,y,z) axes are (a,b,c), respectively. The free-space polarizability along the η-axis can be approximated by

$$\alpha_\eta^{fs} = \frac{\varepsilon_r - \varepsilon_b}{\varepsilon_b + L_\eta(\varepsilon_r - \varepsilon_b)} \frac{abc}{3}, \tag{7}$$

where

$$L_\eta = \frac{abc}{2} \int_{s=0}^{\infty} \frac{1}{(s+r_\eta^2)\left[(s+a^2)(s+b^2)(s+c^2)\right]^{0.5}} ds. \tag{8}$$

In order to include the effects of radiative damping and dynamic depolarization due to the finite size of NPs, the polarizability coefficient, Eq. (7), is modified as,

$$\alpha_\eta^{mlwa} = \left(\frac{1}{\alpha_\eta^{fs}} - i\frac{2}{3}k^3 - \frac{k^2}{r_\eta} \right)^{-1}, \tag{9}$$

which is called as Modified Long Wavelength Approximation (MLWA) [22]. However for NPs in a multilayered medium, the polarizability should be even further modified in order to take layered medium into account as explained in [59]

$$\alpha_\eta^{lm} = \left(\frac{1}{\alpha_\eta^{fs}} - i\frac{2}{3}k^3 - \frac{k^2}{r_\eta} - G_{\eta\eta}^{refl}(\mathbf{r_0}, \mathbf{r_0}) \right)^{-1}, \tag{10}$$

where $\mathbf{r_0}$ is the mass center of the nanoparticle.

4. Numerical Results

In [40, 49, 50], Crozier *et al.* present a systematic study on the dispersion relations of a metal nanoparticle chain fabricated on top of an indium tin oxide coated (ITO) glass slide. For the experiment, they use cylindrical gold nanoparticles with heights of 55 nm, diameters of 90 nm, and center-to-center distances of 140 nm along the length of the chain. The thickness of ITO-coating is 20 nm. The experiment results indicate that *S*-polarized illumination couples to a single mode (transverse, $T1$) and *P*-polarized illumination couples to a single mode (longitudinal, L) at normal incidence, with an additional mode (transverse, $T2$) coupled at large angles of incidence. They conclude that this weak mode only occurs for *P*-polarized light at high incidence angles and it can be associated with nanoparticle dipole moment oriented perpendicular to the substrate. Figure 3 summarizes the results found in [40] for L and $T1$ modes. In [40], they apply CDA technique to calculate SPR modes: by first assuming point dipoles exist in the air (blue lines in Fig. 3), then in the glass (green lines in Fig. 3). It is observed that experimentally obtained dispersion results (dark grey dots) lay in between these two cases.

We analyze the same structure theoretically using layered medium CDA (abbreviated as LM-CDA). For the optical constants of gold, the experimental values are used [60] rather than Drude model to eliminate any concern regarding the selection of appropriate values for plasmon and relaxation frequencies. We model cylinders as ellipsoids and calculate their polarizability using Eq. (10). The refractive indices of glass, ITO and air are assumed to be 1.51, 1.45 and 1, respectively, and the procedure described in the previous section is followed on the complex ω domain using 20 NPs.

Prior to giving complete picture for the dispersion relations calculated with LM-CDA, let us put them together with classical CDA results to demonstrate the improvement

#121182 - $15.00 USD Received 8 Dec 2009; revised 4 Jan 2010; accepted 11 Jan 2010; published 14 Jan 2010

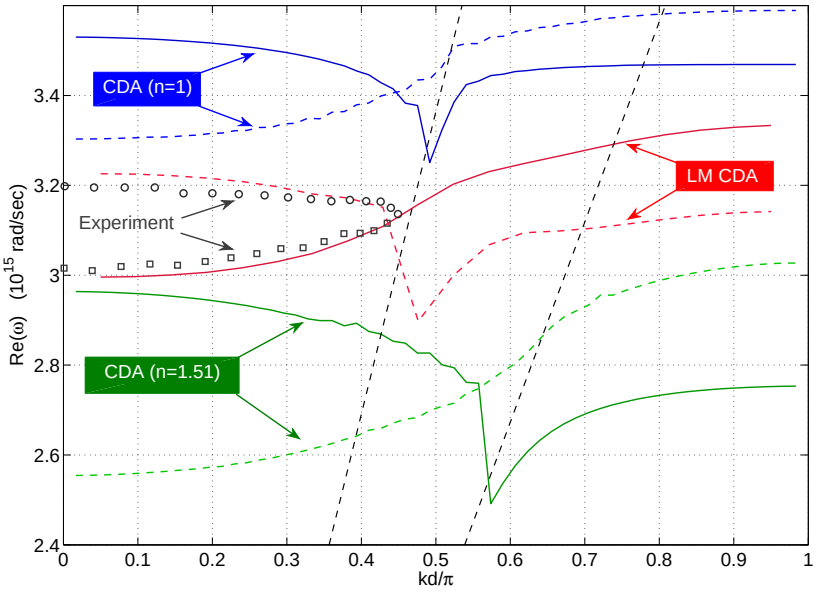

Fig. 3. Experimentally (dark grey circles and squares depict L and $T1$ modes, respectively) and theoretically calculated dispersion curves. Dark blue solid line and light blue dashed line show the CDA results for the transverse and longitudinal modes, respectively, assuming NPs situated in air; green lines assuming NPs situated in glass, red lines assuming NPs embedded on top of an ITO-coated glass slide. Dashed black lines depict light lines in air and glass.

in point dipole modeling from classical CDA to LM-CDA. In Fig. 3, dark red solid line and light red dashed line show the LM-CDA results for the first transverse and the longitudinal modes, respectively, assuming NPs embedded on top of an ITO-coated glass slide. Clearly, (i) there is a very good agreement between the experimental and LM-CDA results, (ii) LM-CDA results are more accurate than the classical CDA and ERI-CDA results (the maximum error is less than 1 % for the LM-CDA, whereas maximum error of CDA implemented with the effective refractive index approximation, abbreviated as ERI-CDA, is about 2.6 % [41]). We can safely say that the use of LMGF and an appropriate polarizability factor is enable us to understand the effect of multilayered background on the dispersion relations for dipolar modes propagating along a chain of metal NPs.

Figure 4 provides a detailed picture of the dispersion relations: Fig. 4 (a) compares experimental (red circles) and theoretical (solid lines) results for the longitudinal mode. Blue and green solid lines depict the real and imaginary parts of the resonance frequencies, respectively. Dashed black lines are light lines in air and glass. Similar to the free space case, for the longitudinal mode there is no sharp interaction with the light line, since longitudinal photons cannot propagate along the chain. The lossy nature of the gold causes large imaginary components for the resonance modes.

Figure 4 (b) repeats (a) for the first transverse mode. Because of the phase matching condition between the free photon and the dipolar chain mode, the first transverse mode is strongly perturbed when $k_{mode} \approx \omega/c$.

In Figure 4 (c), real and imaginary parts of the resonance frequencies are shown for

#121182 - $15.00 USD Received 8 Dec 2009; revised 4 Jan 2010; accepted 11 Jan 2010; published 14 Jan 2010

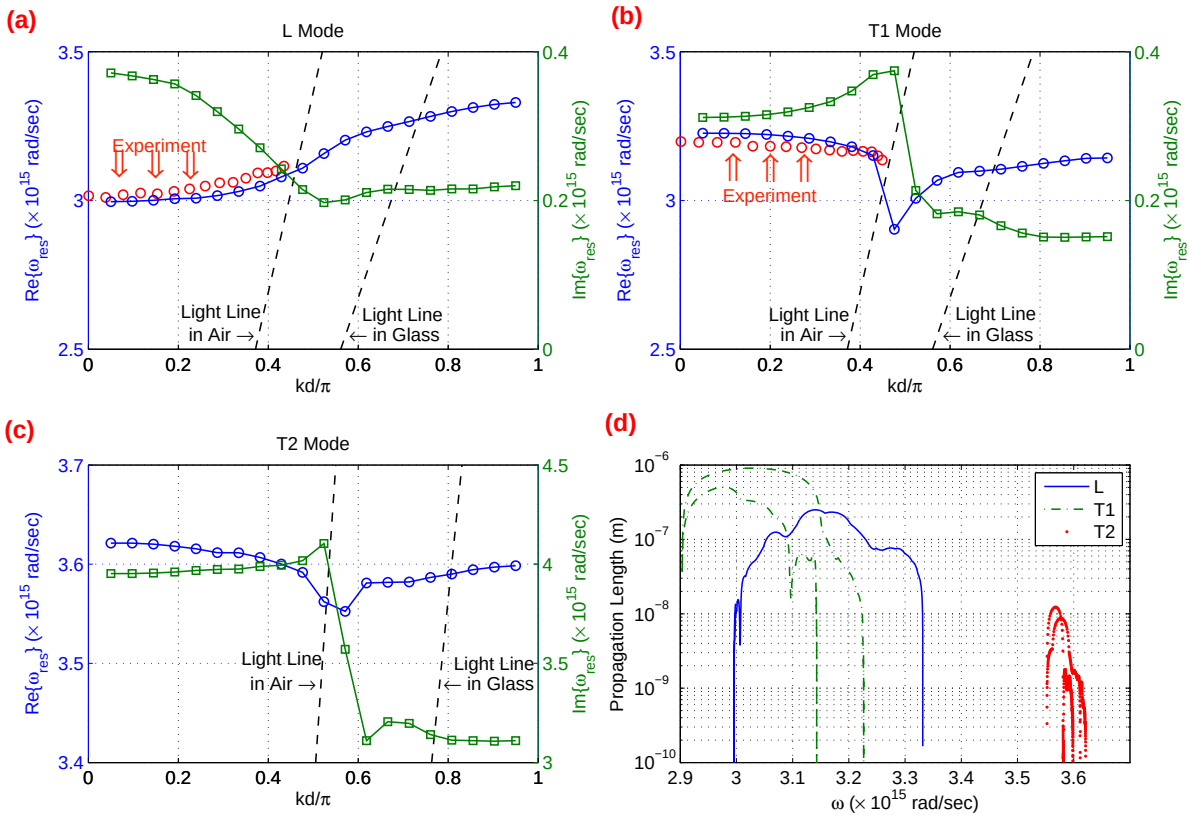

Fig. 4. Dispersion curves for (a) longitudinal, (b) first transverse, (c) second transverse excitation modes, respectively, for the **gold** nanoparticles with heights of 55 nm, diameters of 90 nm, and center-to-center distances of 140 nm along the length of the chain. Nanoparticles are aligned on top an ITO coated glass. The thickness of ITO-coating is 20 nm. Red dots in (a) and (b) are experimental results [40]. Dashed black lines in (a), (b), and (c) depict light lines in air and glass. (d) Propagation lengths derived from the dispersion curves for each mode.

the second transverse mode. As it is also shown in [41], the second transverse mode also interacts strongly with the light line (when $k_{mode} \approx \omega/c$), damping rates diverge near the light line for both transverse modes.

Note that both L and $T1$ modes develop a bandwidth approximately 25 % larger than the case NPs situated in air, resulting in higher group velocities; whereas $T2$ mode's bandwidth is much narrower than the bandwidth of the free space transverse mode.

Thus, another important outcome of these results is on the propagation lengths and group velocities supported by this structure. Figure 4 (d) shows the propagation lengths of each mode derived from the dispersion curves. The maximum propagation length that can be obtained with this structure is around 900 nm (and max. group velocity is around $0.38c$) for the first transverse mode. Since the longitudinal mode does not interact with the light line, dispersion has a smooth shape, and, hence the propagation lengths are much shorter than the ones belonging to the first transverse mode. As it would be expected from the resonance frequencies with very large imaginary components, the

#121182 - $15.00 USD Received 8 Dec 2009; revised 4 Jan 2010; accepted 11 Jan 2010; published 14 Jan 2010

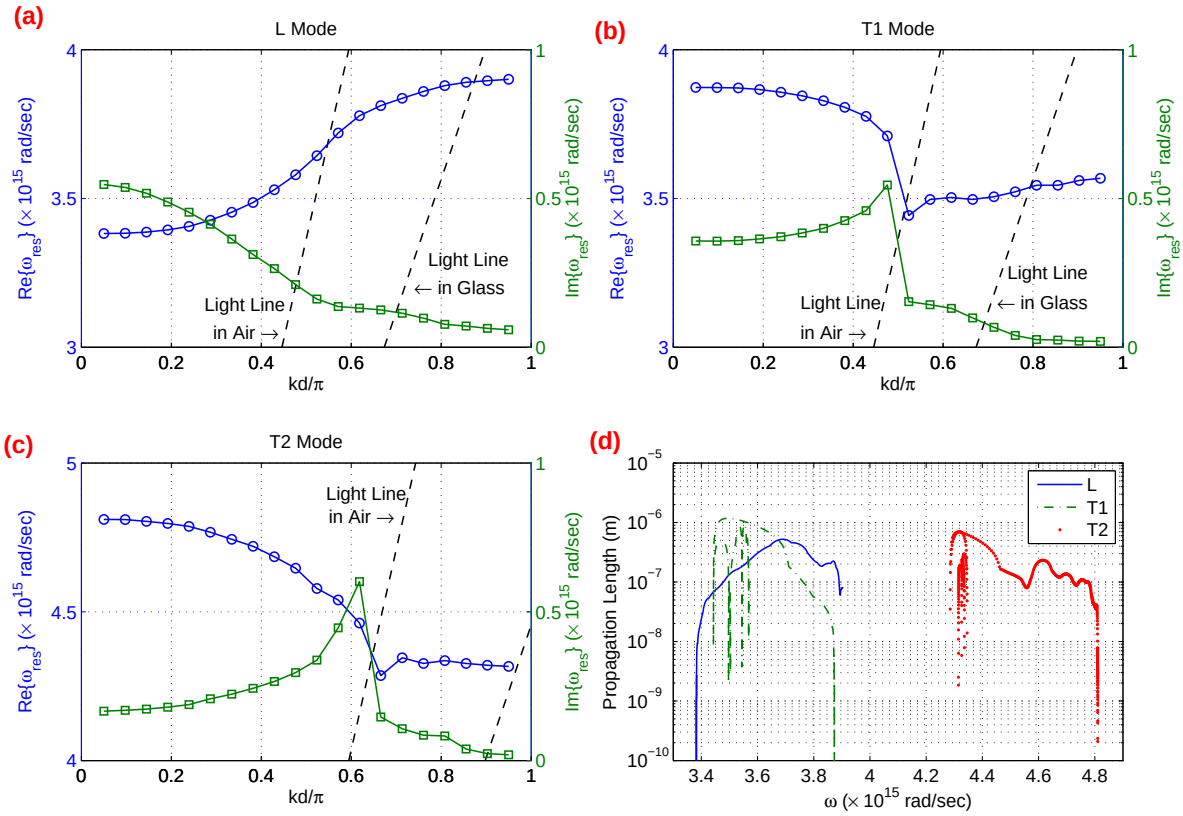

Fig. 5. Dispersion curves for (a) longitudinal, (b) first transverse, (c) second transverse excitation modes, respectively, for the **silver** nanoparticles with heights of 55 nm, diameters of 90 nm, and center-to-center distances of 140 nm along the length of the chain. Nanoparticles are aligned on top an ITO coated glass. The thickness of ITO-coating is 20 nm. (d) Propagation lengths derived from the dispersion curves for each mode.

propagation length of the second transverse mode is even shorter than L and $T1$ modes.

The same numerical study is repeated for the silver NPs. All the parameters are same as the one described above, except the material type of NPs. Fig. 5 shows the dispersion curves and propagation lengths for each mode. Similar to the previous case, radiative losses decrease as we increase the k for the modes below the light line. However, the damping rates are smaller for the chain of silver NPs than the chain of gold NPs, especially below the light line, and hence longer propagation lengths can be achieved using silver NPs (for the first transverse mode, maximum propagation length is about 1.1 μm). Another interesting observation is that maximum propagation lengths of different modes are close to each other for silver NPs, whereas this is not true for gold NPs as shown in Fig. 4 (d).

#121182 - $15.00 USD Received 8 Dec 2009; revised 4 Jan 2010; accepted 11 Jan 2010; published 14 Jan 2010

5. Conclusion

We developed a fully-retarded theoretical model for surface plasmons on metal nanoparticle chains and arrays embedded in a multilayered medium. Polarizability of metal nanoparticles are approximated analytically by taking multilayered medium into account. Numerical results show (i) a very good agreement with the experimental results found in the literature, (ii) the existence of two different transverse modes that strongly couple with light, (iii) propagation lengths around 1 μm are possible in multilayered medium as in the free space case.

6. Acknowledgements

We acknowledge useful discussions with Prof. Vadim A. Markel from University of Pennsylvania. This research was supported by a Marie Curie International Reintegration Grant within the 7^{th} European Community Framework Programme. Contract No. PIRG05-GA-2009-247876.

#121182 - $15.00 USD Received 8 Dec 2009; revised 4 Jan 2010; accepted 11 Jan 2010; published 14 Jan 2010